Kinetic Monte Carlo simulation of faceted islands in heteroepitaxy using a multistate lattice model

Chi-Hang Lam

Department of Applied Physics, Hong Kong Polytechnic University, Hung Hom, Hong Kong, China

(Received 26 August 2009; revised manuscript received 30 October 2009; published 23 February 2010)

A solid-on-solid model is generalized to study the formation of Ge pyramid islands bounded by (105) facets on Si(100) substrates in two dimensions. Each atomic column is not only characterized by the local surface height but also by two deformation state variables dictating the local surface tilt and vertical extension. These local deformations phenomenologically model surface reconstructions in (105) facets and enable the formation of islands which better resemble faceted pyramids. We apply the model to study a kinetic limited growth regime. Transitions from stepped mounds into faceted islands under deposition conditions are demonstrated. It is shown that a significantly reduced growth rate after faceting leads to a continuous nucleation of new islands until overcrowding occurs. The island size distribution is now dominated by fluctuations in the initial island size during faceting and the increased diversity in the ages of the islands. This multistate model may find applications in kinetic simulations of other nanostructures or nanoclusters involving arbitrary high-index surfaces.

DOI: 10.1103/PhysRevE.81.021607 PACS number(s): 81.10.−h, 68.65.Hb, 81.16.Dn, 81.16.Rf

I. INTRODUCTION

Strain induced self-assembly of three-dimensional (3D) islands in heteroepitaxy have been attracting much research interest because of the rich physics involved and their potential applications as quantum dots in optoelectronic devices [1–3]. A widely studied system is Ge deposited on Si(100) substrates with a 4% lattice misfit. Relatively flat islands in the form of stepped mounds with unfaceted sidewalls called prepyramids start to emerge at 3 monolayers (ML) of Ge coverage [4,5]. Further deposition leads to pyramids or rectangular-based huts bounded by (105) facet planes. Deposition temperatures lower than 500 °C generally favors rectangular huts [6,7], while higher temperature often leads to pyramids [8]. After still further deposition or annealing, pyramids can grow into dome islands bounded mainly by steeper (113) facets [9,10].

(105) facets on pyramids and huts have been found to be extraordinarily stable and atomically flat from first-principles calculations [11–14]. At low temperature, surface steps on (105) facets are rarely observed [7]. They are however present at higher temperature and the bunching of them are observed to be important to the morphological evolution [15]. The structures, energies, and dynamics of these steps have been studied using first-principles calculations [16]. Also, the edge energies of a (105) faceted ridge have been estimated using molecular-dynamics simulations based on empirical potentials [17].

Large scale simulations of the formation of 3D islands is possible using kinetic Monte Carlo (KMC) methods based on lattice models [18–27]. The simulations are computationally very intensive due to the long-range nature of elastic interactions. Using advanced algorithms, simulations adopting realistic elastic interactions in two-dimensional (2D) [21,22] and 3D [23–26] with, respectively, large and moderate system sizes have become possible. With more approximate forms of effective elastic interactions, larger systems in 3D can also be studied [20,27].

KMC studies on strained layers are generally based on square or cubic lattices for simplicity. Strain induced islands or pits are readily generated but their sidewalls are almost vertical [18,24,26] or at an inclination of about 45° [19,21,23,27] depending on the details of the bond energies or additional constraints used. These inclinations are much steeper than 11° and 26° for the (105) and (113) facets, respectively. The realistic facets however are of rather low symmetry and in general are not favored energetically in lattice models. Besides quantitative errors, it is possible that this discrepancy in the surface inclination may even lead to qualitatively different growth modes in certain situations. Furthermore, the surface energy of the island sidewalls from existing KMC models are not independently adjustable and there is no simple approach to incorporate for example the extraordinary stability of certain facets. With only one favored sidewall slope in a given model, only one type of island can be simulated so that studying the pyramid to dome transition [15] for instance is impossible.

In this work, we extend the convectional ball and spring lattice model for KMC simulation of heteroepitaxial solids in 2D by allowing specific geometrical deformation states of the surface atoms. These deformations phenomenologically represent surface reconstructions on (105) facets. We apply this multistate model to simulate the deposition of strained layers at 450 °C. The formation of faceted islands from stepped mounds is studied and the impact of this shape transition on the island size distribution is explored. We also demonstrate qualitative differences in the island nucleation and coarsening dynamics between faceted and unfaceted islands.

II. BALL AND SPRING LATTICE MODEL

We first explain the conventional square lattice model of elastic solids in 2D while further extensions will be introduced in the next section. Every atom is associated with a lattice site and are connected to nearest and next nearest

neighbors by elastic springs. Solid-on-solid conditions are assumed. We follow the model parameters used in Ref. [21] unless otherwise stated to approximate the widely studied Ge/Si(001) system. We assume a substrate lattice constant $a_s=2.715$ Å so that a_s^3 gives the correct atomic volume in crystalline silicon. The lattice misfit $\epsilon=(a_f-a_s)/a_f$ equals 4%, where a_f is the lattice constant of the film. Nearest and next-nearest neighboring atoms are directly connected by elastic springs with force constants $k_N=13.85$ eV$/a_s^2$ and $k_{NN}=k_N/2$, respectively. The elastic couplings of adatoms with the rest of the system are weak and are completely neglected for better computational efficiency. In this model, surface steps have a particularly high tendency to bunch together under strain presumably due to the much weaker entropic surface step repulsion in 2D. We hence forbid double surface steps as well as adjacent single surface steps of the same direction so that the steepest surface slope allowed is 1/2.

The KMC approach simulates the morphological evolution by explicitly considering the diffusion of surface atoms. Every topmost atom m on the film can hop to a nearby site with a hopping rate $\Gamma(m)$ following an Arrhenius form:

$$\Gamma(m) = R_0 \exp\left[\frac{-n_m\gamma + \Delta E_s(m) + E_0}{k_B T}\right], \tag{1}$$

where n_m is the number of nearest and next-nearest neighbors of atom m. We have assumed an identical nearest and next-nearest neighbor bond strength γ. We put $\gamma=0.5$ eV, slightly larger than the value in Ref. [21] so that the energy costs of stepped mounds become slightly higher. The energy $\Delta E_s(m)$ is the difference in the strain energy E_s of the whole lattice at mechanical equilibrium with or without the atom m. Due to the long-range nature of elastic interactions, its efficient calculation is highly nontrivial and we handle it using a Green's-function method together with a super-particle approach explained in Refs. [21,25,28]. In addition, $E_0=3\gamma-0.67$ eV, where 0.67 eV is the adatom diffusion barrier on the (100) plane. The hopping barrier as given in Eq. (1) is hence $(n_m-3)\gamma-\Delta E_s(m)+0.67$ eV. To speed up the simulations, long jumps are allowed so that a hopping atom will jump directly to another random topmost site at most $s_{max}=8$ columns away with equal probability. Then, $R_0=2D_0/(\sigma_s a_s)^2$, with $D_0=3.83\times10^{13}$ Å^2 s^{-1} and $\sigma_s^2=\frac{1}{6}(s_{max}+1)(2s_{max}+1)$. This gives the appropriate adatom diffusion coefficient for silicon (100).

III. MULTISTATE LATTICE MODEL WITH SURFACE DEFORMATION

To effectively model (105) facets, which are more precisely (15) surfaces in 2D, we introduce additional degrees of freedom representing local deformations to all topmost atoms. They phenomenologically accounts for the surface rebonding or reconstruction states on a (105) faceted region [11]. Therefore, while all atoms admit nonlocal deformation due to the long-range misfit stress, the topmost atoms may further be locally deformed. For efficient computation, these deformations localized to individual surface atoms are assumed to be completely independent of the misfit induced nonlocal deformation although correlations between misfit strain and surface reconstruction are known to exist [12–14]. In the following calculation of the local deformation energies, we thus neglect lattice misfit. The independent calculation of the misfit strain energy term is identical to that outlined in Sec. II.

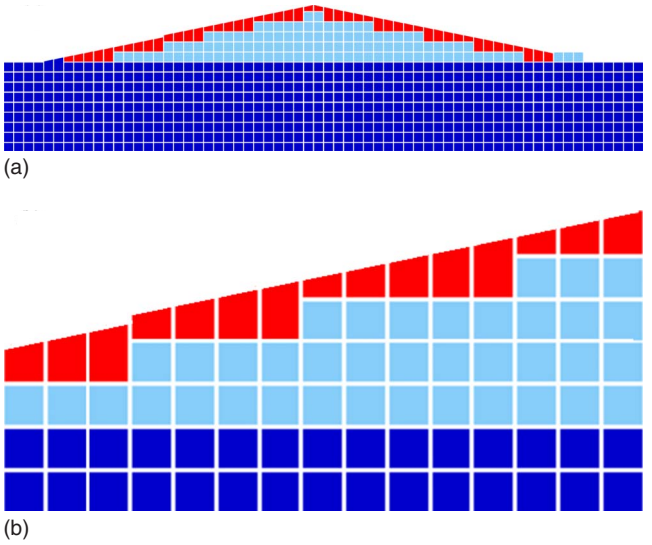

FIG. 1. (Color online) A faceted island from a small scale simulation using the multistate model (a) and a magnification of part of the surface containing a (105) surface step between the third and the fourth columns (b). Locally deformed film atoms, locally undeformed film atoms and all substrate atoms are shaded in red, light blue, and dark blue, respectively. Misfit induced strain is not illustrated. In (b), the tilt variable σ_i is $\frac{1}{5}$ for all columns, while the extension variable κ_i from left to right equals $0,\frac{1}{5},\frac{2}{5},-\frac{1}{5},0,\frac{1}{5},\frac{2}{5},-\frac{2}{5},-\frac{1}{5},0,\frac{1}{5},\frac{2}{5},-\frac{2}{5},-\frac{1}{5}$, and 0.

We first show an example of a faceted island from a small scale simulation in Fig. 1(a). Figure 1(b) magnifies part of the surface. It shows how the surface deformation smoothes out the (100) steps of the original stepped mound and turn the sidewalls into atomically flat effective (105) facets with slopes $\pm1/5$. An example of a surface step on the (105) surface is also shown and will be explained later. We express all lengths in unit of the lattice constant. In the absence of deformation, an atom is represented by a unit square. An integer h_i denotes the surface height at column i. We assume that a topmost atom in the film surface or in an exposed region of the substrate can be deformed into a trapezoid characterized by two deformation state variables, namely, a tilt variable σ_i and an extension variable κ_i. We put

$$\sigma_i = 0, \frac{1}{5}, \quad \text{or} \quad -\frac{1}{5}, \tag{2}$$

which gives the slope of the upper surface of the deformed atom. The values $\sigma_i=\pm1/5$ enable the formation of the (105) facets in both directions. As shown in Fig. 1(b), attaining a flat (105) faceted region further requires properly coordinated vertical stretching or compression of the topmost atom by κ_i which is given by

$$\kappa_i = \begin{cases} 0 & \text{for } \sigma_i = 0 \\ -\frac{2}{5}, -\frac{1}{5}, 0, \frac{1}{5}, \text{ or } \frac{2}{5} & \text{for } \sigma_i = \pm\frac{1}{5}. \end{cases} \quad (3)$$

The ith atomic column hence can be rectangular or trapezoidal with the left and right edges of heights h_i^a and h_i^b given by

$$h_i^a = h_i + \kappa_i - \frac{\sigma_i}{2}, \quad (4)$$

$$h_i^b = h_i + \kappa_i + \frac{\sigma_i}{2}. \quad (5)$$

A surface step in between the ith and the $(i+1)$th column has a step height δ_i defined as

$$\delta_i = |h_{i+1}^a - h_i^b|. \quad (6)$$

For simplicity, we have measured step heights as projected along the lattice axis rather than the surface normals. Note that single steps on (100) and (105) surfaces have very different heights of 1 and 1/5, respectively.

We will next explain the energy cost of the local deformations of the surface atoms. Values of the energy parameters to be introduced are chosen phenomenologically to provide morphologies best compared with observations. Similar to the original lattice model [21], although we believe that our parameters are within physically acceptable ranges, this model being in 2D is not realistic enough to apply directly parameters from first-principles studies in general. Furthermore, we have found from numerous exploratory simulations that only a rather limited and specific range of parameters provides reasonable morphologies under a wide range of relevant growth conditions. The constraints on our parameters hence may also shed light on how the morphologies reveals certain features on the microscopic details of the surface and this will be discussed further.

The hopping rate of a topmost atom m in Eq. (1) is generalized to

$$\Gamma(m) = R_0 \exp\left[\frac{\Delta E_b(m) + \Delta E_s(m) + E_0'}{k_B T}\right], \quad (7)$$

where $E_0' = -\gamma - 0.67$ eV. The misfit strain energy term $\Delta E_s(m)$ is defined similarly as before and its calculation is assumed to be completely independent of the local surface deformation as explained above. The surface energy term $\Delta E_b(m)$ denotes the change in the bond energy E_b of the whole surface when the site is occupied versus unoccupied. Surface energy is defined relative to that of a flat (100) surface as

$$E_b = \sum_i [\phi(\sigma_i) + \psi(\sigma_i, \sigma_{i+1}) + \omega(\delta_i, \sigma_i, \sigma_{i+1})]. \quad (8)$$

Here, $\phi(\pm 1/5) = 5$ meV is the formation energy per site of the (105) facet and $\phi(0) = 0$ for the (100) region. If we choose a larger value of $\phi(\pm 1/5)$, the (105) facet can become unstable. Also, $\psi(\sigma_i, \sigma_{i+1}) = 0.35$ eV denotes the interface energy at the boundary of a facet where $\sigma_i \neq \sigma_{i+1}$ and it is zero otherwise. It dictates the energy barrier of facet nucleation. A negative value of the site formation energy $\phi(\pm 1/5)$ has been suggested [14] corresponding to extremely stable (105) facets. However, this is not acceptable as island sizes from such simulations are then dominated by ψ which is closely related to the edge energy in Ref. [14] but is practically independent of the lattice misfit.

The last term in Eq. (8) represents the energy of a surface step. On a (100) region with $\sigma_i = \sigma_{i+1} = 0$, it is defined as

$$\omega(\delta_i, \sigma_i, \sigma_{i+1}) = \frac{\gamma}{2}\delta_i, \quad (9)$$

where the step height δ_i defined in Eq. (6) is an integer. This results from simple bond counting noting that two single steps are created by breaking one nearest neighboring bond of strength γ. Noting also that both nearest and next-nearest neighboring bonds have strength γ so that a bulk atom has a bond energy of -4γ, Eqs. (7)–(9) reduces exactly to Eq. (1). A (100) region in the multistate model thus behaviors identically to that in the basic model in Sec. II. Outside of a (100) region (i.e., σ_i or $\sigma_{i+1} \neq 0$) we put

$$\omega(\delta_i, \sigma_i, \sigma_{i+1}) = \beta_{105}(1 + \chi - \chi e^{1-5\delta_i}) + \frac{\gamma}{2}\left(\delta_i - \frac{1}{5}\right), \quad (10)$$

for $\delta_i \geq 1/5$ and it is zero otherwise. This expression gives an energy β_{105} for a single step with height $\delta_i = 1/5$ on a (105) region. It is known that incomplete (105) facets can be practically absent at low temperature around 450 °C [7] but are observable at 550 °C [15]. We reproduce this feature in our model by taking a relatively large value of $\beta_{105} = 0.3$ eV. From Eq. (10), the step energy per unit height of a multiple step approaches $\gamma/2$ identical to that on a (100) facet. This also reduces the energy of an adatom on a (105) surface which is bounded by two unit steps to a more acceptable but still very large value of 1.3 eV. The parameter χ determines the energy of multiple steps of intermediate heights. We put $\chi = 0.5$ allowing a slight tendency of step bunching [15].

In KMC simulation using this multistate model, the atomic hopping events are randomly sampled and simulated according to the rate $\Gamma(m)$ in Eq. (7). We assume that the deformation state variables σ_i and κ_i at every column are unchanged after an atomic hop, i.e., the deformation state is attached to the column rather than to the hopping atom. Deposition of an atom also increases the column height by unity without altering the deformation state. After every period τ, the deformation state for a set of columns will be updated. Specifically, to facilitate program parallelization, we adopt a sublattice updating scheme in which the deformation states at all odd (even) lattice sites will be updated at every odd (even) updating event. When column i is to be updated, the variables σ_i and κ_i are resampled from the allowed set of 11 possible combinations given in Eq. (3) corresponding to $(\sigma_i, \kappa_i) = (0,0), (\pm 1/5, \pm 2/5)$, $(\pm 1/5, \pm 1/5)$, and $(\pm 1/5, 0)$ using a heat bath algorithm based on the relative probability $\exp(-E_b/kT)$. We take $\tau = 2/\Gamma_{ad}$, where Γ_{ad} is the adatom hopping rate on a (100) surface easily calculable from Eq. (1). At 450 °C, $\tau \simeq 2.30 \times 10^{-7}$ s. Local changes in the surface reconstruction states are most likely a fast process compared with atomic hopping.

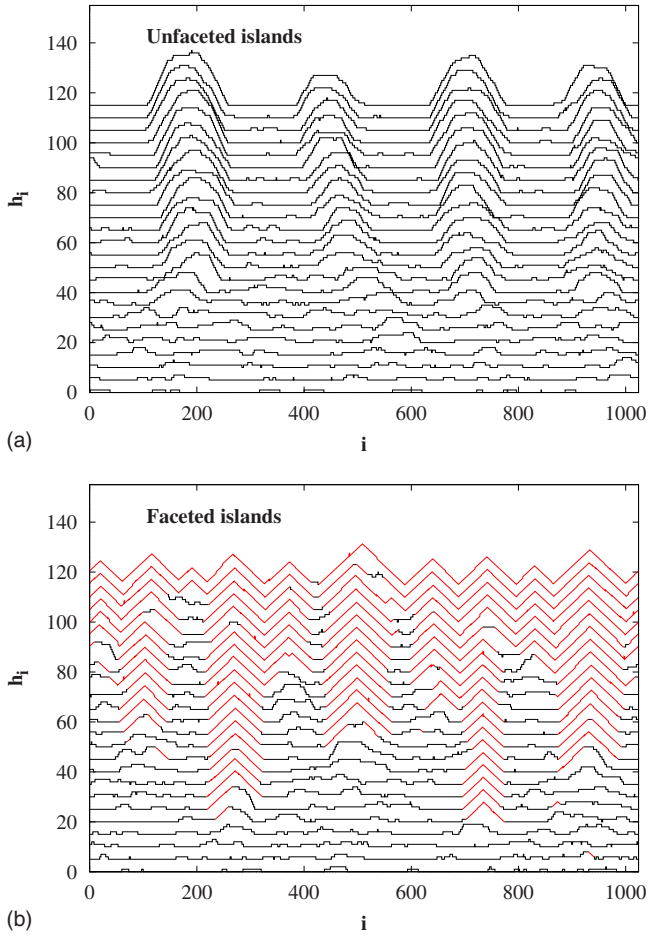

FIG. 2. (Color online) Snapshots of surfaces taken after the deposition of every 1/4 ML up to a thickness of 6 ML showing the development of (a) unfaceted and (b) faceted islands simulated respectively using the conventional model and the multistate model. (105) faceted regions are shaded in red. Each successive profile is displaced upward by five units vertically.

We have checked that our deformation state updating rate is indeed sufficiently fast so that a further increase in the updating rate gives no observable difference to our results. This adopted rate is also the highest possible rate without increasing significantly the overall execution time of our program. Our model follows detailed balance which allows us to confirm the reliability of our software implementation using a Boltzmann's distribution test [25].

IV. RESULTS

Using both the conventional ball and spring lattice model and the multistate lattice model with surface deformation explained in Secs. II and III, we have simulated the self-assembly of strained islands in 2D. A substrate of size 1024×1024 (width $\times$ depth) is used. We take a temperature 450° and a deposition rate 0.1 ML/s. The conventional and the multistate models lead to islands with unfaceted and faceted sidewalls, respectively. For convenience, we refer to them as unfaceted and faceted islands.

Figure 2(a) shows the evolution of unfaceted islands from a typical run using the conventional model during deposition of up to 6 ML of film material on to an initially flat substrate. The plotted profiles are taken after the deposition of every 1/4 ML and have been displaced vertically for clarity. Unstable shallow stepped mounds develop at very early stage. After depositing about 2 ML, some stepped mounds have attained steeper sidewalls and become more stable. At about 4 ML, they have generally attained the steepest possible slope of 1/2 allowed in our model. As observed in this and other similar runs, there is a rather well defined island nucleation period and no new island emerges after some larger islands are well established. We also observe that some relatively mature islands eventually decay and vanish, indicating a coarsening process. The existence of a finite nucleation period followed by coarsening is consistent with previous KMC simulations [27] as well as continuum simulations [29,30]. It has more direct experimental relevance at higher temperature although the pyramid to dome transition and alloying between the film and substrate atoms [10] add further complications.

Analogous evolution of faceted islands simulated using the multistate model with surface deformation is shown in Fig. 2(b). Small highly unstable (105) faceted regions with deformed surface atoms begin to appear at a coverage of about 0.5 ML. Relatively stable (105) faceted islands emerge at about 1 ML. These islands develop from the larger ones of the stepped mounds. Faceted regions nucleate on either side of the mounds independently so that half faceted asymmetric islands exist during the course of development. Islands also often go through an truncated pyramid stage [5] with unfaceted tops before finally becoming fully developed pyramids. Some faceted islands may occasionally decay partially or even completely back to unfaceted stepped mounds, but the larger ones are much more stable. On the other hand, some stepped mounds may happen to get faceted at rather small sizes while slightly larger ones can remain unfaceted for long periods. Therefore, the faceting process under the current growth conditions is strongly affected by both energetics and kinetics.

At this low growth temperature of 450°, surface steps on a (105) facet is rare as explained in Sec. III. Further growth of faceted islands by step flow is hence kinetic limited [6,7]. It can be observed from Fig. 2(b) that island growth slows down dramatically once becoming faceted. Their sizes occasionally jump up rapidly only when parts of the sidewalls become temporarily unfaceted due to thermal excitations. Since faceted islands are poor absorber of newly deposited atoms, new islands continue to nucleate until the substrate is crowded with islands.

For more quantitative analysis, we define an island as one in which each of the constituent columns must be at least four atoms tall. All islands can then be automatically identified. Figure 3 traces the size evolution against the nominal film thickness h of every island in Fig. 2 once they have attained a size of at least 150 atoms. Islands from another similar run are also included in Fig. 3(a) to provide additional examples. From Fig. 3(a), unfaceted islands beyond a certain size in general grow steadily with its own characteristic rates which are expected to depend mainly on the sizes of their adatom capture zones. Small islands decay and van-

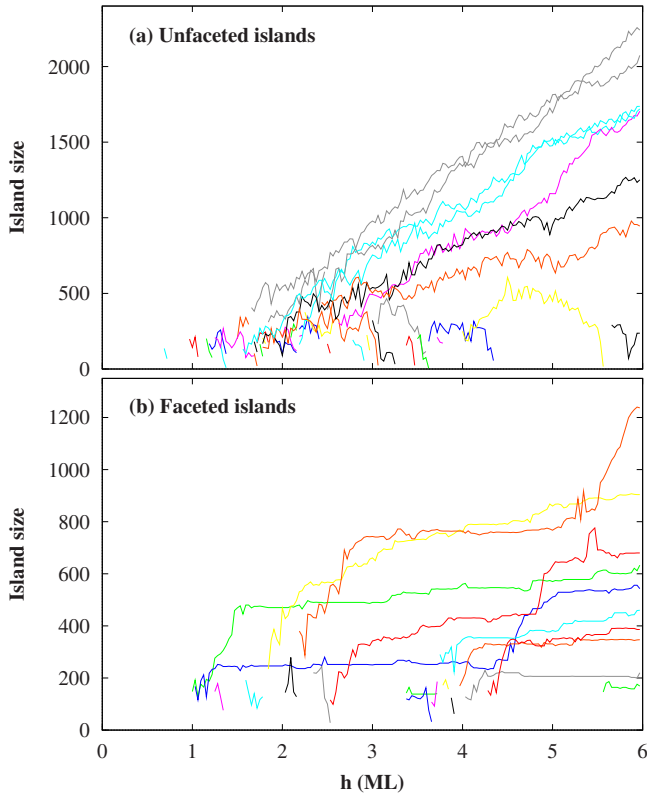

FIG. 3. (Color online) Plot of individual island size against nominal film thickness h for unfaceted (a) and faceted (b) a set of typical islands showing relatively steady and intermittent growth, respectively.

ish. Fluctuations in the growth rates are often associated with thermally activated geometrical fluctuations of individual islands. For example, islands taking less stable geometries can lose atoms rapidly either one by one as adatoms or in groups as detached subcritical islands. In contrast, from Fig. 3(b), there is in general an initial period of rapid island growth followed by much slower growth after faceting. Once faceted, their sizes remain nearly constant except at occasional jumps associated with temporary partial decay of the facets as described above.

To obtain more statistics, we have conducted very large scale simulations by repeating each simulation 200 times. A single run takes about 10 h to complete on a 2.6 GHz dual core personal computer. Figure 4 plots the average number of islands of size 150 or larger on a 1024 atoms wide substrate used. Smaller islands are excluded because they are highly unstable. For unfaceted islands, their number first increases indicating a period of active nucleation at coverage from about 1 to 2.5 ML. It then declines but at a very slowly rate indicating rather inefficient coarsening as deposition continues. In contrast, faceted islands steadily increase in number for coverage up to about 5 ML due to continuous nucleation. Beyond 5 ML, the substrate is crowded with islands and the number of islands saturates.

We have histogrammed the island sizes from all the independent runs. Figure 5 plots the average number of islands on the substrate against island size n. For both models, a peak island size emerges for $h \gtrsim 2.5$ ML. For unfaceted islands, the histogram broadens significantly upon further growth mainly due to a wide distribution of growth rates. The width of the distribution however increases slightly slower than the average island size $\bar{n}$. The distribution of the scaled island size $n/\bar{n}$ hence gradually narrows. We believe

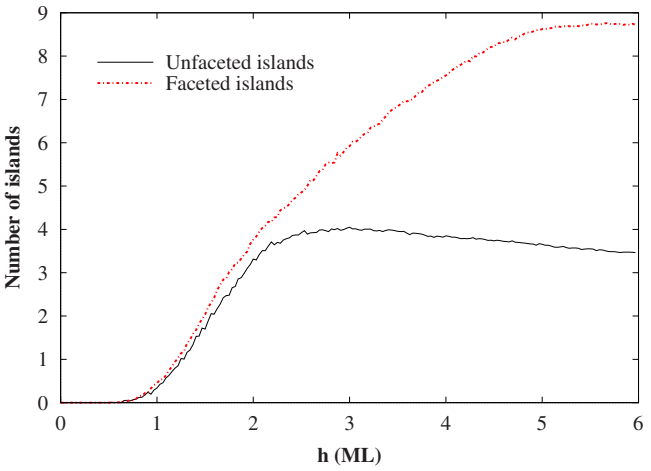

FIG. 4. (Color online) Plot of the number of islands on a substrate of 1024 atoms wide against nominal film thickness h averaged over 200 independent runs in each case.

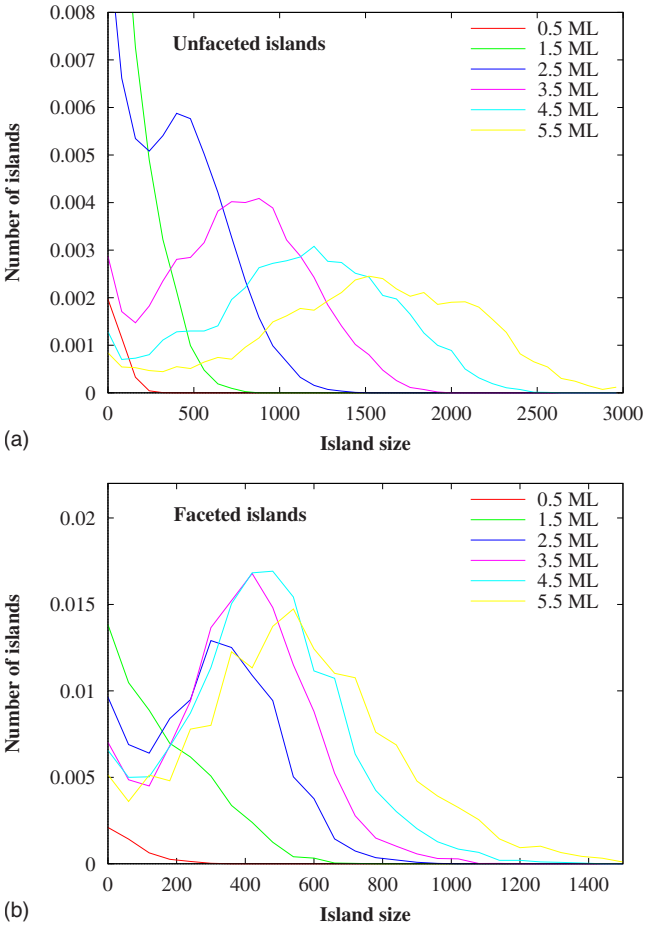

FIG. 5. (Color online) Size histograms for unfaceted (a) and faceted (b) islands.

that this narrowing results mainly from the decay of the smaller islands. Island statistics for the case of irreversible homoepitaxial growth has been extensively studied [31,32] (see Ref. [33] for a review). The size distribution for the current reversible heteroepitaxial case is much less understood. Beyond 3 ML, the distribution observed here reasonably resembles those reported previously from reversible submonolayer growth in 3D systems [34,35]. It can also be roughly approximated by empirical forms for irreversible growth in which a trimer is the smallest stable island (i.e., $i=2$ in Ref. [31]). In contrast for faceted islands, it broadens much more slowly due to the highly kinetic limited growth mode. Nevertheless, the faceted islands do not possess narrower size distribution relative to the average size. This is because a significant size distribution already exists when the islands become faceted as can be observed in Fig. 2(b). The continuous nucleation of new islands also broadens the distribution as the older islands are larger on average. Another difference between the models is that the peak of the histogram decays monotonically upon deposition for unfaceted islands while it increases for $2.5 \leq h \leq 4.5$ due to the continuous nucleation of islands.

To better understand the origin of the island size distribution, the growth rates of individual islands are studied. Figure 6 plots of the island growth rate dn/dt against the island size n at a coverage of 3 ML for all islands having attained a size of at least 150 atoms. No ensemble averaging is performed. Each value of island size is averaged over 32 measurements on the same island taken at various nominal film thickness $h=2.5-3.5$ ML. The growth rate is obtained by comparing similar temporally averaged size of a given island measured at nominal film thickness $h=3-3.5$ ML with that at $h=2.5-3$ ML corresponding to an average time lapse of 5 s noting the deposition rate being 0.1 ML/s. For unfaceted islands [Fig. 6(a)], despite strong random fluctuations among islands, there is a clear trend of correlation between island growth rate and the island size. Larger islands in general tends to grow faster as expected in typical coarsening processes. A small population of islands of small sizes shrinks despite the deposition flux. Other factors should also contribute to the correlation since for instance a large capture zone can enhance the growth rate and thus at the same time also the island size. For faceted islands in Fig. 6(b), the dependence is at most very weak. This implies that coarsening is strongly suppressed in the kinetic limited regime and is consistent with the findings from the size histogram evolution explained above.

We have also computed the width of the adatom capture zone of every island which is defined here in 2D as the mean distance of its center of mass from those of its left and right neighbors. The size of the capture zone is known to be directly related to the island growth rate in irreversible homoepitaxial island growth and its distribution have been extensively studied [36–38]. Figure 7 replots the same data on the island growth rate but this time against the capture zone width w. Island grow rates in general deviate significantly from the expectation wR with R being the deposition rate 0.1 ML s^{-1} which assumes simple incorporation of new atoms solely according to the capture zone. This is consistent with previous experimental findings on Ge islands grown at

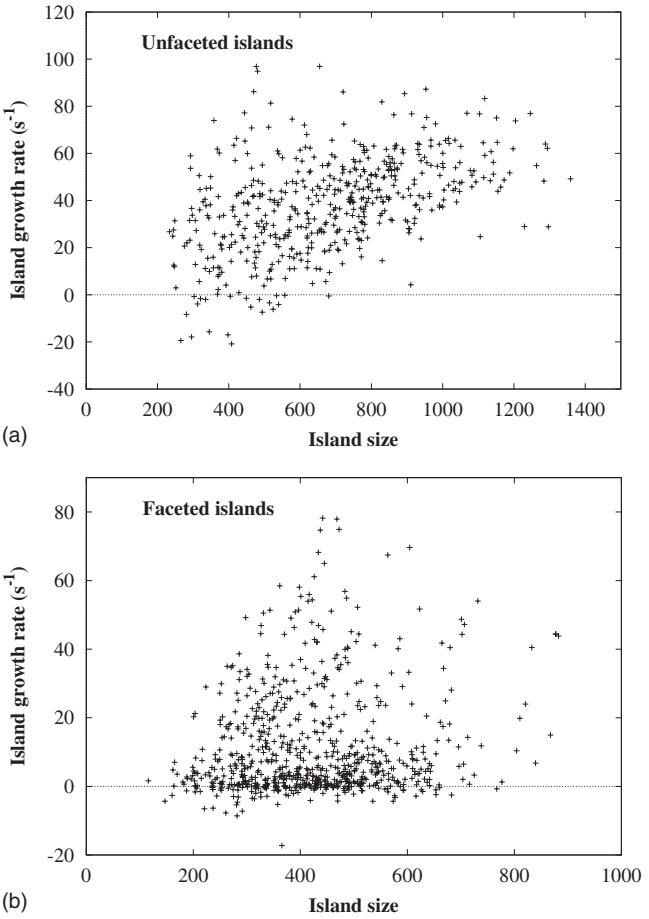

FIG. 6. Plot of growth rate against size for all unfaceted (a) and faceted (b) islands having reached a size of at least 150 atoms at nominal film thickness $h=3$ ML.

620 °C [39]. Island growth is hence far from being a simple diffusion limited process. Fluctuations and coarsening are also important. Furthermore, the dependence of the growth rate on the capture zone size is weak for unfaceted islands [Fig. 7(a)] and is completely absent for faceted islands [Fig. 7(b)]. For faceted islands, the growth rate is therefore largely independent of both its size and the capture zone width and again reveals that its growth in the kinetic limited regime is essentially randomly activated.

V. DISCUSSIONS

The multistate model proposed here has allowed the successful simulation of the transition of initially unfaceted stepped mounds into (105) faceted pyramid islands. This is an atomistic simulation on the formation of this high-index surface. In contrast, conventional lattice model only generates high symmetry surfaces while the computationally far more intensive *ab initio* and molecular-dynamics approaches are limited to basically static studies.

This new model allows us to study island growth in the kinetic limited regime computationally which has not been possible before. In this regime, island growth slows down dramatically and becomes intermittent after faceting. The

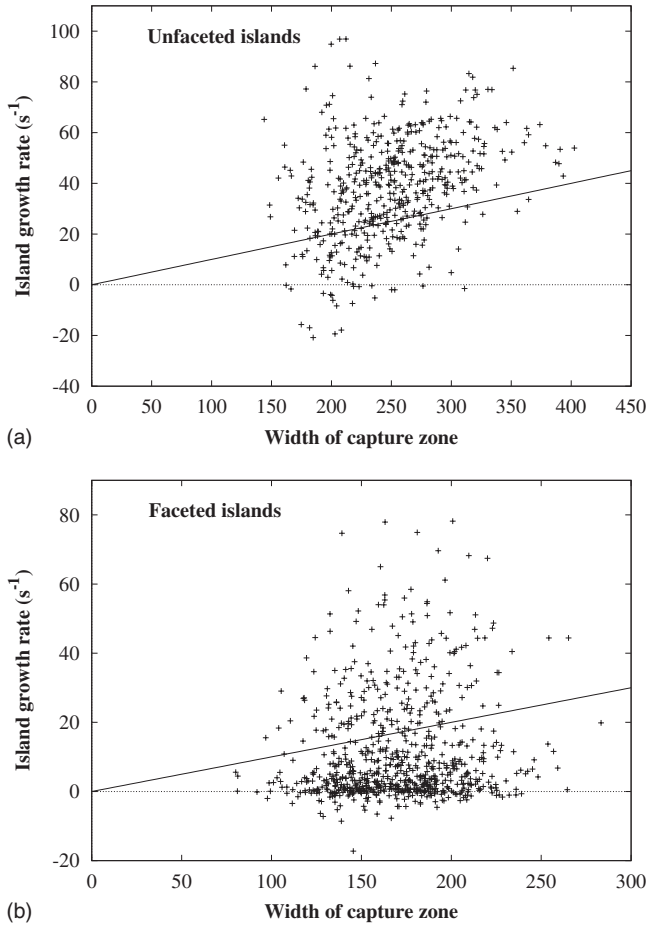

FIG. 7. Plot of growth rate against width of island capture zone using the same date as in Fig. 6. The solid lines indicate expected growth rate based on the width the capture zone alone.

slower growth of the more established islands also leads to a continuous nucleation of islands until the substrate is fully occupied. Deposition experiments at 550 °C do indicate slower growth of matured islands and a continuous island nucleation growth mode [8]. Our work shows that continuous island nucleation is a consequence of kinetic limited growth.

Uniformity of the island sizes is a highly desired property for potential quantum dot application of the islands. It is known that the pyramid to dome shape transition can reduce island size distribution as the lower energy of the transformed state leads to the rapid consumption of smaller untransformed islands [40]. In our study, the mound to pyramid transition could also potentially generates more uniform islands at the critical size since the much slower pyramid growth rate nearly halt the island growth. Nevertheless, the large ensemble fluctuations in the shape transition size severely limits the size uniformity. Furthermore, continuous island nucleation also leads to increased diversity in the island ages. This results in further size broadening since faceted islands grows continuously despite relatively slowly. The identification of this factors may shed light on how to reduce to the size distribution in this regime.

The evolution of island sizes have been studied theoretically using mean-field-type equations [40,41]. A more detailed theory accounting for the spatial correlation of the islands should also consider the evolution of the island capture zones using for example rate equations well established for homoepitaxial growth [42]. The stochastic nature of the growth is also very important. Fluctuations in the deposition flux, adatom exchanges between islands, upper layer and facet nucleation events, and those induced by geometrical excitations of islands should in principle be accounted for.

It is straight forward to generalize our model to include still more facet types. This has enabled us to perform atomistic dynamic simulation of the pyramid-to-dome transition. The island transition size and the transition energy barrier are also studied [43]. Such simulation had been impossible with conventional lattice model. More generally, our multistate formalism allows the generalization of the widely used solid-on-solid models to describe arbitrary facet types phenomenologically. It may be generalized to study the evolution of other strained or unstrained nanostructures or nanoclusters involving high-index surfaces.

In summary, we have generalized a lattice model for strained films to allow a set of local surface deformation states of surface atoms representing effective surface reconstructions. These local deformations are assumed to be independent of the misfit induced strains. Using this multistate lattice model, we have performed kinetic Monte Carlo simulations in 2D. Stepped mounds first emerge and then transform spontaneously into faceted islands. We have studied the kinetic limited growth regime and observed a continuous nucleation of islands until overcrowding occurs. From large-scale simulations, we have extensively studied statistical properties including island density, size distributions, and island growth rates. For faceted islands, they characterize kinetic limited growth with coarsening strongly suppressed. In contrast, using the conventional lattice model, unfaceted islands in the form of stepped mounds exhibit a simple nucleation period followed by continuous growth and gradual coarsening.

ACKNOWLEDGMENT

This work was supported by HK RGC, Grant No. PolyU-5009/06P.

[1] P. Politi, G. Grenet, A. Marty, A. Ponchet, and J. Villain, Phys. Rep. **324**, 271 (2000).
[2] V. A. Shchukin, N. N. Ledentsov, and D. Bimberg, *Epitaxy of Nanostructures* (Springer, New York, 2003).
[3] I. Berbezier and A. Ronda, Surf. Sci. Rep. **64**, 47 (2009).
[4] Y.-W. Mo, D. E. Savage, B. S. Swartzentruber, and M. G. Lagally, Phys. Rev. Lett. **65**, 1020 (1990).
[5] A. Vailionis, B. Cho, G. Glass, P. Desjardins, D. G. Cahill, and J. E. Greene, Phys. Rev. Lett. **85**, 3672 (2000).
[6] M. Kästner and B. Voigtländer, Phys. Rev. Lett. **82**, 2745 (1999).
[7] M. R. McKay, J. A. Venables, and J. Drucker, Phys. Rev. Lett. **101**, 216104 (2008).
[8] A. Rastelli and H. von Kanel, Surf. Sci. **532-535**, 769 (2003).
[9] G. Medeiros-Ribeiro, A. Bratkovski, T. Kamins, D. Ohlberg, and R. Williams, Science **279**, 353 (1998).
[10] A. Rastelli, M. Stoffel, J. Tersoff, G. S. Kar, and O. G. Schmidt, Phys. Rev. Lett. **95**, 026103 (2005).
[11] Y. Fujikawa, K. Akiyama, T. Nagao, T. Sakurai, M. G. Lagally, T. Hashimoto, Y. Morikawa, and K. Terakura, Phys. Rev. Lett. **88**, 176101 (2002).
[12] S. Cereda, F. Montalenti, and L. Miglio, Surf. Sci. **591**, 23 (2005).
[13] G.-H. Lu, M. Cuma, and F. Liu, Phys. Rev. B **72**, 125415 (2005).
[14] O. Shklyaev, M. Beck, M. Asta, M. Miksis, and P. Voorhees, Phys. Rev. Lett. **94**, 176102 (2005).
[15] F. Montalenti *et al.*, Phys. Rev. Lett. **93**, 216102 (2004).
[16] S. Cereda and F. Montalenti, Phys. Rev. B **75**, 195321 (2007).
[17] C. M. Retford, M. Asta, M. J. Miksis, P. W. Voorhees, and E. B. Webb III, Phys. Rev. B **75**, 075311 (2007).
[18] B. G. Orr, D. Kessler, C. W. Snyder, and L. Sander, Europhys. Lett. **19**, 33 (1992).
[19] K. E. Khor and S. Das Sarma, Phys. Rev. B **62**, 16657 (2000).
[20] M. Meixner, E. Scholl, V. Shchukin, and D. Bimberg, Phys. Rev. Lett. **87**, 236101 (2002).
[21] C.-H. Lam, C.-K. Lee, and L. M. Sander, Phys. Rev. Lett. **89**, 216102 (2002).
[22] J. L. Gray, R. Hull, C.-H. Lam, P. Sutter, J. Means, and J. A. Floro, Phys. Rev. B **72**, 155323 (2005).
[23] M. T. Lung, C.-H. Lam, and L. M. Sander, Phys. Rev. Lett. **95**, 086102 (2005).
[24] G. Russo and P. Smereka, J. Comput. Phys. **214**, 809 (2006).
[25] C.-H. Lam, M. T. Lung, and L. M. Sander, J. Sci. Comput. **37**, 73 (2008).
[26] J. Y. Lee, M. J. Noordhoek, P. Smereka, H. McKay, and J. M. Millunchick, Nanotechnology **20**, 285305 (2009).
[27] R. Zhu, E. Pan, and P. W. Chung, Phys. Rev. B **75**, 205339 (2007).
[28] C.-H. Lam and M. T. Lung, Int. J. Mod. Phys. B **21**, 4219 (2007).
[29] P. Liu, Y. Zhang, and C. Lu, Phys. Rev. B **68**, 035402 (2003).
[30] J.-N. Aqua, T. Frisch, and A. Verga, Phys. Rev. B **76**, 165319 (2007).
[31] J. G. Amar and F. Family, Phys. Rev. Lett. **74**, 2066 (1995).
[32] M. Bartelt and J. Evans, Surf. Sci. **298**, 421 (1993).
[33] J. Evans, P. Thiel, and M. Bartelt, Surf. Sci. Rep. **61**, 1 (2006).
[34] M. Petersen, C. Ratsch, R. E. Caflisch, and A. Zangwill, Phys. Rev. E **64**, 061602 (2001).
[35] C. Ratsch, J. DeVita, and P. Smereka, Phys. Rev. B **80**, 155309 (2009).
[36] P. A. Mulheran and J. A. Blackman, Phys. Rev. B **53**, 10261 (1996).
[37] A. Pimpinelli and T. L. Einstein, Phys. Rev. Lett. **99**, 226102 (2007).
[38] F. Shi, Y. Shim, and J. G. Amar, Phys. Rev. E **79**, 011602 (2009).
[39] S. Miyamoto, O. Moutanabbir, E. E. Haller, and K. M. Itoh, Phys. Rev. B **79**, 165415 (2009).
[40] F. M. Ross, J. Tersoff, and R. M. Tromp, Phys. Rev. Lett. **80**, 984 (1998).
[41] H. T. Dobbs, D. D. Vvedensky, A. Zangwill, J. Johansson, N. Carlsson, and W. Seifert, Phys. Rev. Lett. **79**, 897 (1997).
[42] P. A. Mulheran and D. A. Robbie, Europhys. Lett. **49**, 617 (2000).
[43] C.-H. Lam, e-print arXiv:0912.0053.